Mon. Not. R. astr. Soc. (1988) **232,** 339–360

Tidal torques and local density maxima

Alan Heavens *Department of Astronomy, University of Edinburgh, Blackford Hill, Edinburgh EH9 3HJ*

John Peacock *Royal Observatory, Blackford Hill, Edinburgh EH9 3HJ*

Accepted 1987 November 16. Received 1987 November 16; in original form 1987 September 7

Summary. We have calculated the distribution of tidal torques acting on matter in the neighbourhood of local density maxima when the density perturbations are small. We find that high peaks experience higher torques than low peaks. The higher torques acting on the high peaks are counteracted by the shorter collapse time during which the torques can act. Which effect is dominant depends on the perturbation power spectrum: for power spectra characteristic of both cold dark matter and hot dark matter, the effects nearly cancel, and the total angular momentum acquired by a collapsing object is almost independent of the height of the peak. Furthermore, the distributions of angular momenta acquired by collapsing protosystems are extremely broad, for all power spectra; the range of angular momenta of peaks of a given height far exceeds any modest systematic differences between peaks of different height.

We have also calculated the distribution of λ – the dimensionless spin parameter – for density maxima. This quantity has a median value $\lambda \simeq 0.05$ with no strong dependence on power spectrum, in good agreement with N-body simulations. Unlike total angular momentum, λ does show an anticorrelation with peak height, but again the distributions are very broad by comparison with the systematic shift.

These results indicate that it is not possible to account for the systematic differences in angular momentum properties of disc and elliptical galaxies simply by postulating that the latter arise from fluctuations of greater overdensity, contrary to some recent suggestions.

1 Introduction

In models of galaxy formation relying on gravitational instability, the notion that angular momentum arises as a result of tidal torques has been around for some time (Hoyle 1949). However, it is only comparatively recently that a fairly complete description of the process has appeared in Western literature (White 1984). Expanding an analysis of Doroshkevich (1970), White showed explicitly how the first-order tidal gravitational field couples with the zero-order

anisotropy of a collapsing object to produce a first-order torque. This results in the angular momentum of the proto-object growing to first-order (in terms of, say, the fractional density perturbation $\delta\varrho/\varrho$), and proportional to time. The apparently contradictory second-order growth found by Peebles (1969) arises only as a result of the choice of a Lagrangian sphere as the proto-object.

In order to follow the growth of angular momentum in the later stages of collapse ($\delta\varrho/\varrho \geqslant 1$), N-body simulations must at present be employed (e.g. Efstathiou & Jones 1979; Efstathiou & Barnes 1983). Recently, Barnes & Efstathiou (1987) have completed an extensive study of angular momentum growth in collapsing systems, and conclude that linear theory is not always a reliable technique for determining the final angular momentum of a collapsed object (although see the criticisms of this conclusion by Hoffman 1988). Analytic studies of this problem are in any case not yet complete, and do have the advantage (recognized by Barnes & Efstathiou) of being able to treat exceptional objects which occur only rarely in numerical studies.

In this paper, we calculate the tidal torques acting on the material in the neighbourhood of local density maxima in the linear regime, using the techniques pioneered by Doroshkevich (1970) and extended by Peacock & Heavens (1985) and Bardeen *et al.* (1986) (see also Couchman 1987). The principal assumption involved is that the density field at early times is Gaussian noise – the usual assumption for models where structure forms the gravitational instability of small density perturbations. Such an approach would not be applicable in models where explosions (e.g. Ostriker & Cowie 1981; Ikeuchi 1981) or cosmic strings (e.g. see Vilenkin 1985 for a review) are the principal ingredients of galaxy formation.

We are particularly interested in the effect of the overdensity (or 'height') of the peak on the angular momentum of the collapsing object. It has been argued (Blumenthal *et al.* 1984; Hoffman 1986) that the height of a peak is anticorrelated with its angular momentum, on the basis that very overdense peaks collapse early, so there is not much time for the tidal torques to act. However, such an effect was not seen in the N-body experiments performed by Barnes & Efstathiou; we believe this is because the argument ignores any systematic dependence of the *magnitude* of the tidal torques on the height of the peak. This paper demonstrates that there is such a systematic effect; high peaks do experience greater tidal torques, counteracting somewhat the shorter time during which the torques effectively act. For realistic power spectra, the two effects very nearly cancel.

The second important result of this paper is that the distributions of angular momenta are very broad. Although there are differences between the most likely angular momentum of peaks of different heights, such differences are generally rather small in comparison with the spread in the angular momentum distribution for a given peak height. This is consistent with the results of Barnes & Efstathiou.

The outline of the paper is as follows: in Section 2 we calculate the angular momentum of the material in the neighbourhood of a local density maximum, in terms of local quantities evaluated at the peak itself. The distribution of these quantities is calculated in Appendix A, and Appendix B translates this into distributions of angular momenta for peaks of different height, with asymptotic results being given in Appendix C. Applications of these results in practice are considered in Section 3, and Section 4 summarizes the paper.

2 Angular momentum around a density peak

2.1 TIDAL TORQUES

The angular momentum of the material in a volume around a local density maximum is

$$J_i = a^4 \varepsilon_{ijk} \int \varrho(\mathbf{r}, t)(r - r_{\rm pk})_j (v - v_{\rm pk})_k \, d^3\mathbf{r} \qquad (1)$$

where the subscript pk indicates quantities evaluated at the local maximum, and $a(t)$ is the cosmic scale factor, normalized to unity at the present epoch; $\mathbf{r}$ is therefore a comoving coordinate. Employing a Taylor expansion for the velocity field $\mathbf{v}$, and expanding to first-order in small quantities,

$$J_i = a^4 \varepsilon_{ijk} \varrho(t) v_{kl} \int (r-r_{\rm pk})_j (r-r_{\rm pk})_l \, d^3\mathbf{r} \tag{2}$$

where $\varrho(t)$ is the average density of the Universe at time t, and $v_{kl} \equiv (\partial v_k/\partial r_l)_{\rm pk}$. The main difficulty with analytic calculations like this is to decide what matter eventually ends up in the bound system associated with the peak. We shall assume that the relevant criterion is that the nearby matter be above a certain overdensity threshold, i.e. $\delta \equiv \delta\varrho/\varrho > f\delta_{\rm pk} (f \approx 0)$, with δ given by a Taylor expansion about the peak:

$$\delta \simeq \delta_{\rm pk} + \tfrac{1}{2}\delta_{ij}(r-r_{\rm pk})_i (r-r_{\rm pk})_j \tag{3}$$

where δ_{ij} is the second derivative of the overdensity field (evaluated at the peak): the Kronecker delta appears nowhere in this paper. Note that the approximations in equations (2) and (3) will not be strictly valid once $\delta \ll \delta_{\rm pk}$. If we now rotate the coordinate axes to be aligned with the principal axes of the constant-overdensity ellipsoids, then

$$\delta \simeq \delta_{\rm pk} - \tfrac{1}{2}\sigma_2 \sum_1^3 \lambda_i (r-r_{\rm pk})_i^2 \tag{4}$$

where $-\sigma_2\lambda_i$ are the eigenvalues of the second-derivative matrix. σ_m is the $2m$th wavenumber moment of the density fluctuation power spectrum (see Appendix A). The boundary of the integration volume in equation (2) is then given by the solution of

$$2(\sigma_0/\sigma_2)(1-f)\nu_{\rm pk} = \sum_1^3 \lambda_i (r-r_{\rm pk})_i^2 \tag{5}$$

where $\nu_{\rm pk}$ is the height of the peak in units of the rms overdensity, $\sigma_0(t)$. The prescription clearly only makes sense if $\nu_{\rm pk} > 0$. The principal semi-axes of the approximately ellipsoidal surface $\delta = f\delta_{\rm pk}$ are given by

$$a_i^2 = 2\left(\frac{\sigma_0}{\sigma_2}\right)\frac{(1-f)}{\lambda_i}\nu_{\rm pk}. \tag{6}$$

Thus

$$J_i = a^4 \varepsilon_{ijk} g(t) \sigma_0 \varrho(t) \bar{v}_{kl} \int_{-a_m}^{a_m} r_j r_l \, d^3\mathbf{r} \tag{7}$$

where we have chosen $\mathbf{r}_{\rm pk} = \mathbf{0}$ without loss of generality, $g(t) \equiv a(t)\partial(\ln\delta)/\partial t$, and $\bar{v}_{jk}$ is the normalized second-derivative matrix of the peculiar velocity: $\bar{v}_{jk} \equiv v_{jk}/[g(t)\sigma_0(t)]$ (see Appendix A). The unperturbed Hubble expansion does not, of course, contribute to the angular momentum. Integration gives

$$\mathbf{J} = \frac{4\pi}{15} a^4(t) g(t) \varrho(t) \sigma_0(t) a_1 a_2 a_3 ([a_2^2 - a_3^2]\bar{v}_{23}, [a_3^2 - a_1^2]\bar{v}_{13}, [a_1^2 - a_2^2]\bar{v}_{12}) \tag{8}$$

since for growing-mode perturbations, the velocity field is curl-free and $v_{ij} = v_{ji}$. We may separate the time-dependence by writing the magnitude of the angular momentum vector as

$$J(t) \equiv j_e J_{\rm ref}(t) \tag{9}$$

where $J_{\rm ref}(t)$ is the same for all peaks, $j_{\rm e}$ (standing for j at early times) depends on the shape and height of the peak, and varies only slowly with time in the linear regime. The principal time-dependence is via

$$J_{\rm ref}(t) \equiv a(t)\varrho_0 g(t)\sigma_0(t)R_*^5(1-f)^{5/2} \tag{10}$$

where ϱ_0 is the present mean density of the Universe, and

$$R_* \equiv \sqrt{3}(\sigma_1/\sigma_2) \tag{11}$$

is a characteristic comoving length for the power spectrum, normally expressed as a function of the comoving wavenumber k (the factor $\sqrt{3}$ is an arbitrary scaling: we have chosen our notation to

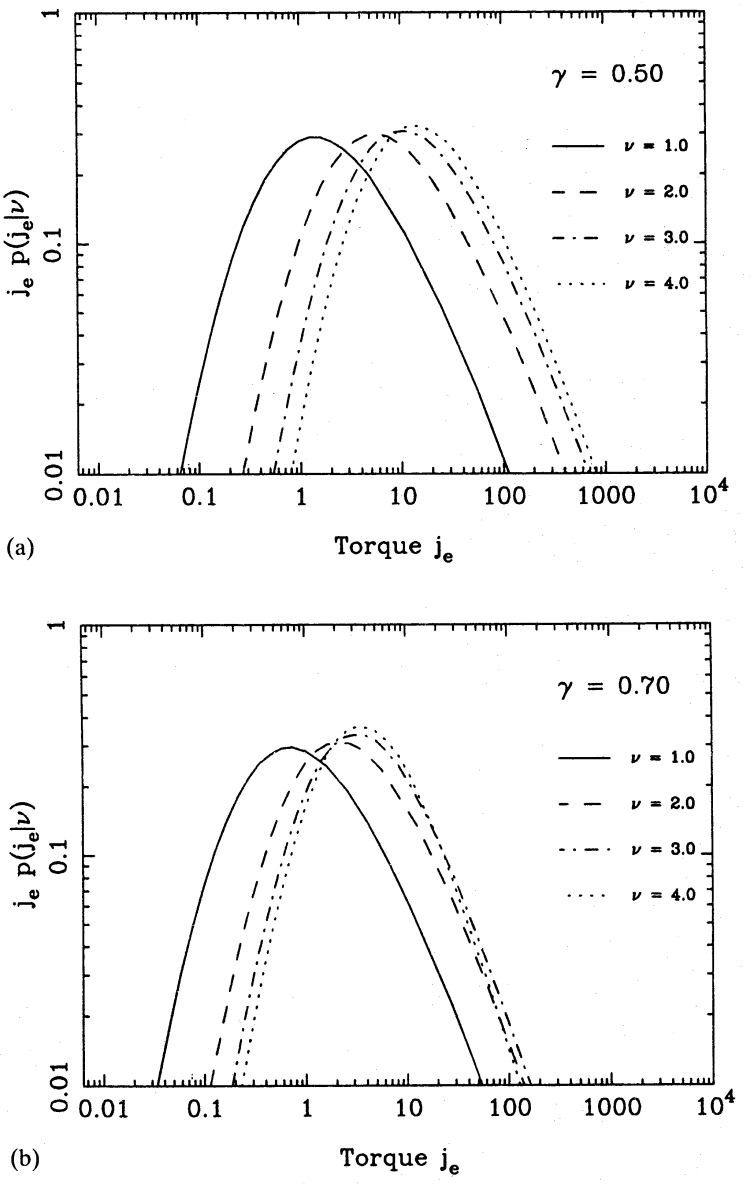

Figure 1. The conditional probability distribution for the angular momentum of material in the vicinity of peaks of heights 1–4 (in units of the rms overdensity, σ_0), at early times. The (time-dependent) unit of $j_{\rm e}$ is given by equation (12). $j_{\rm e}$ effectively measures the tidal torques acting on the material which is near a peak. Fig. 1(a)–(c) show different power spectra. Notice that power spectra with a lot of power on scales much larger than the peak separation (γ=0.5) show a large systematic shift towards higher torques for higher peaks. For steep spectra (γ=0.9), this effect is much less marked, and absent for ν>2.

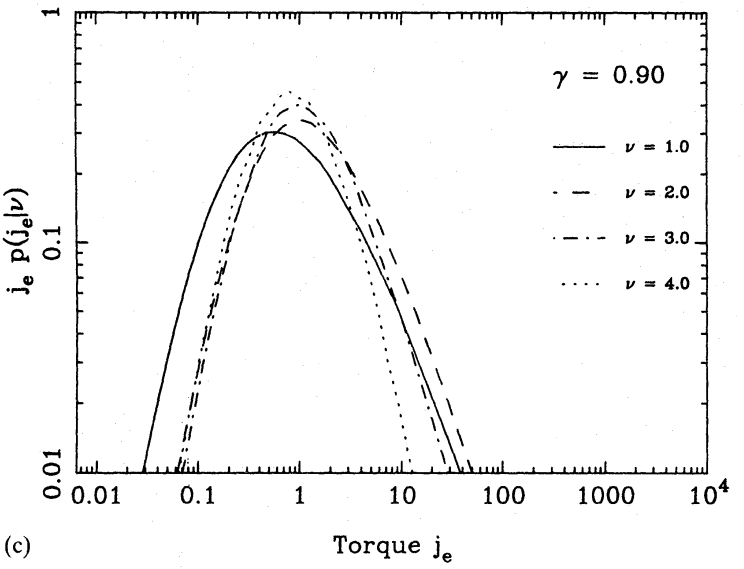

(c)

Figure 1–*continued*

agree with Bardeen *et al.*). Physically, R_* provides a measure of the smallest wavelength in the power spectrum. This may result from damping (as in hot dark matter), or be an artificial windowing by the observer (as is usual in cold dark matter models). The latter may be a desirable feature: in a clustering hierarchy, galaxies will combine into successively larger bound systems. These may be identified approximately by finding peaks in the density field smoothed on larger scales. For an Einstein–de Sitter Universe,

$$J_{\rm ref}(t)=\tfrac{2}{3}\varrho_0\sigma_{00}R_*^5(1-f)^{5/2}\,\frac{t}{t_0^2} \tag{12}$$

growing proportional to t, as found by Doroshkevich (1970) and White (1984). The rms fractional density perturbation is σ_{00} at the present epoch, t_0. The angular momentum grows in this way only until the protosystem breaks away from the expansion and forms a discrete system. After that epoch (t_c), the torques are significantly reduced (Peebles 1969). The dimensionless angular momentum at early times $t\ll t_c$, j_e, is given by

$$j_e=\frac{2^{9/2}\pi\nu^{5/2}}{5\times3^{7/2}\gamma^{5/2}\Lambda^{1/2}}\,(\alpha_1^2w_1^2+\alpha_2^2w_2^2+\alpha_3^2w_3^2)^{1/2} \tag{13}$$

where $\alpha_1\equiv1/\lambda_3-1/\lambda_2$, $\Lambda\equiv\lambda_1\lambda_2\lambda_3$ and $w_1^2\equiv\tilde{v}_{23}^2$ with obvious extensions to other indices, such that $\alpha_i\geqslant0$. We have dropped the pk suffix on the ν. γ is a parameter less than unity characterizing the power spectrum, defined by Bardeen *et al.* as $\gamma\equiv\sigma_1^2/(\sigma_0\sigma_2)$.

In order to calculate the angular momentum distribution, we must first calculate the joint distribution of the shape parameters λ_i and velocity shear terms w_i. This is done in Appendix A. The distribution is given by equation (A22), and is integrated in Appendix B to give a joint distribution for the angular momentum j_e and height ν. This information is plotted in Fig. 1 for peaks of different heights and three power spectra, characterized by the parameter γ. Note that the j_e-distribution is essentially the distribution of tidal torques acting during the time when the density perturbations are small. Since the angular momentum grows as t in an Einstein–de Sitter Universe, the torque is constant, and is related to j_e by

$$\text{torque}=\tfrac{2}{3}\varrho_0\sigma_{00}R_*^5(1-f)^{5/2}t_0^{-2}j_e. \tag{14}$$

Inspection of Fig. 1 shows clearly that high peaks experience somewhat stronger torques, on average, than the low peaks. The stronger torques on high peaks are counteracted by the fact that high peaks collapse earlier than low peaks. We shall return to this shortly, but will first discuss the torque distributions in a little more detail.

The asymptotic limits of the distributions are $N_{\rm pk} \propto j_{\rm e}^2$ ($j_{\rm e} \to 0$) and $N_{\rm pk} \propto j_{\rm e}^{-7/3}$ ($j_{\rm e} \to \infty$) (see Appendix C). The latter limit is interesting; the distribution declines sufficiently gradually with $j_{\rm e}$ that the mean torque barely converges. However, the high-$j_{\rm e}$ systems have $\lambda_3 \approx 0$, i.e. one very long axis, as determined from the eigenvalues of the δ_{ij} matrix at the peak. The approximation that the density is accurately given by the first two terms in the Taylor expansion about the peak will almost certainly break down for these systems, as will the assumption about what matter ends up bound to the collapsed object. Truncation of the longest axis at some multiple of R_* would lead to a cut-off in the distribution of high-$j_{\rm e}$ systems.

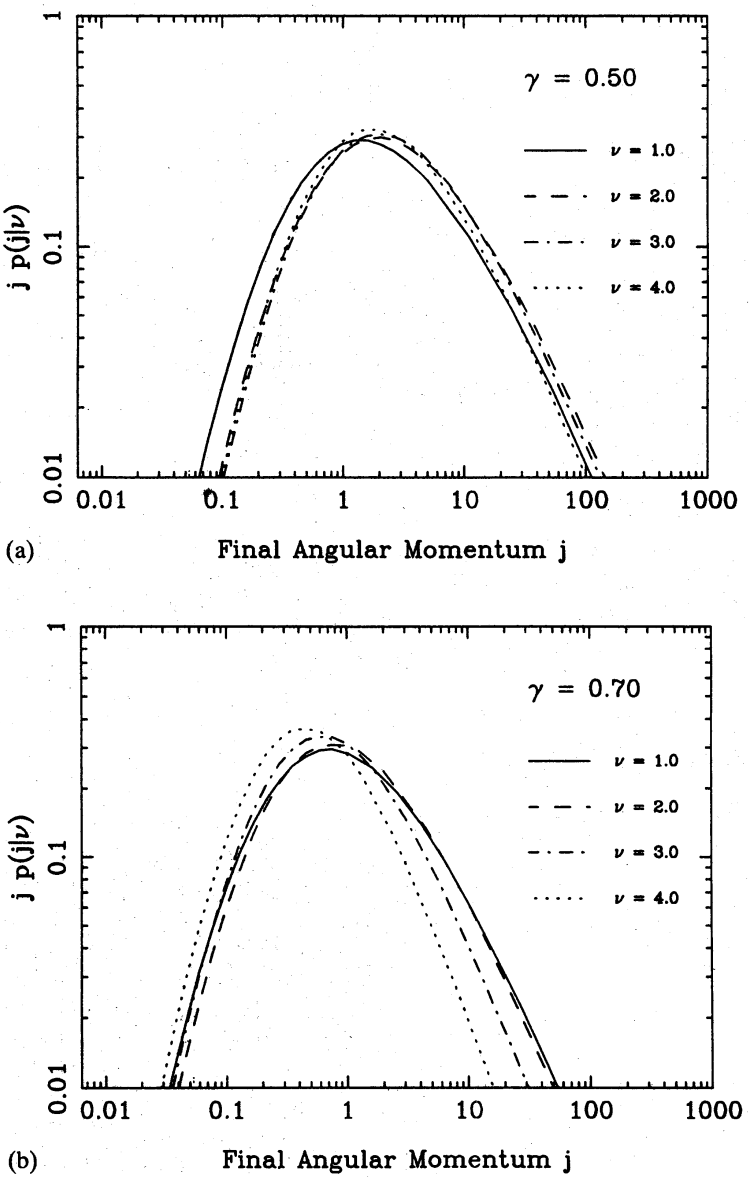

Figure 2. The final angular momentum acquired by peaks of different height, taking into account the shorter collapse times of higher peaks. The number density distributions have been normalized so the figures show probability distributions for j given the peak height. Notice that for $\gamma < 0.7$, there is little systematic dependence of angular momentum with peak height. Notice also that the distributions are very broad.

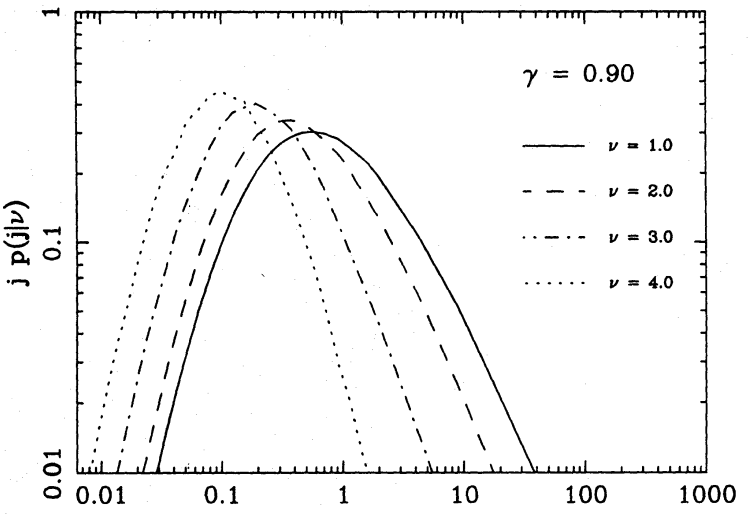

(c)

Figure 2–*continued*

We now return to the question of the final angular momentum acquired by a collapsed object. If we assume that angular momentum growth effectively ceases when $\delta\varrho/\varrho$ reaches a certain value (of order unity), then the time for the torques to act, $t_c(\nu)$, will be closely proportional to $\nu^{-3/2}$ (provided angular momentum growth ceases when the density parameter is not much less than unity). With this assumption, we can calculate the distributions of final angular momentum acquired throughout the collapse, by writing

$$J_{\rm final}(\nu)\equiv J_{\rm ref}[t_c(\nu)]j_e$$

or

$$J\equiv J_{\rm final}(\nu)=J_{\rm ref}[t_c(\nu=1)]\nu^{-3/2}j_e. \tag{15}$$

In other words $J(\nu)=J_{\rm ref,\,f}j$, where

$$j=j_e\nu^{-3/2} \tag{16}$$

and $J_{\rm ref,\,f}$ is defined by the two previous equations. The distribution of j is written down explicitly in Appendix B, but effectively amounts to shifting the j_e distribution to lower j_e by a factor $\nu^{3/2}$. These are shown in Fig. 2. The balance between higher torques and shorter collapse times depends on the power spectrum, via γ. The adiabatic cold dark matter spectrum, when smoothed on galactic scales, has $\gamma\approx0.62$, while a spectrum characteristic of adiabatic neutrino fluctuations with $n=1$ has $\gamma\approx0.73$ (Bardeen *et al.* 1986). In the latter case, the collapsing protosystems are identified with superclusters rather than galaxies. A high value of γ arises from steep fluctuation spectra, whereas a low value indicates a considerable amount of power in fluctuations much larger than the smoothing length.

We see that, for very high values of γ (≈0.9), the higher torques are not sufficient to overcome the short collapse times, and high peaks acquire rather less angular momentum than lower peaks, as postulated by Blumenthal *et al.* (1984) and Hoffman (1986). However, for more realistic power spectra ($\gamma\approx0.6$–0.8), the effect of the higher torques is broadly to balance the shorter collapse times. For very flat spectra ($\gamma<0.6$), the torques on high peaks are so strong that the high peaks acquire more angular momentum than the low peaks. We shall discuss the reasons for this in Section 4.

A good fit to the j distributions is

$$p_{\rm pk}(j|\nu)\cong\frac{7.35}{j_0[(j_0/j)^{2/5}+(j/j_0)^{7/15}]^5} \tag{17}$$

where the single parameter is fitted by

$$j_0(\gamma,\,\nu)=0.27+(\gamma-0.7)(0.325-1.3\nu-0.225\nu^2)+(\gamma-0.7)^2(-2.625+6\nu-1.375\nu^2). \tag{18}$$

Our prescription for determining the epoch at which torques cease to be important is, of course, rather crude. It ignores the modest shape-dependence of collapse times (More, Heavens & Peacock 1986), but it includes the most important effect of peak height. It is probably not justified to use anything more sophisticated, in view of the non-linear effects which are likely to modify the angular momentum in the late stages of collapse. Barnes & Efstathiou (1987) argue that non-linear effects are so large as to render linear theory of little value. This is correct so far as

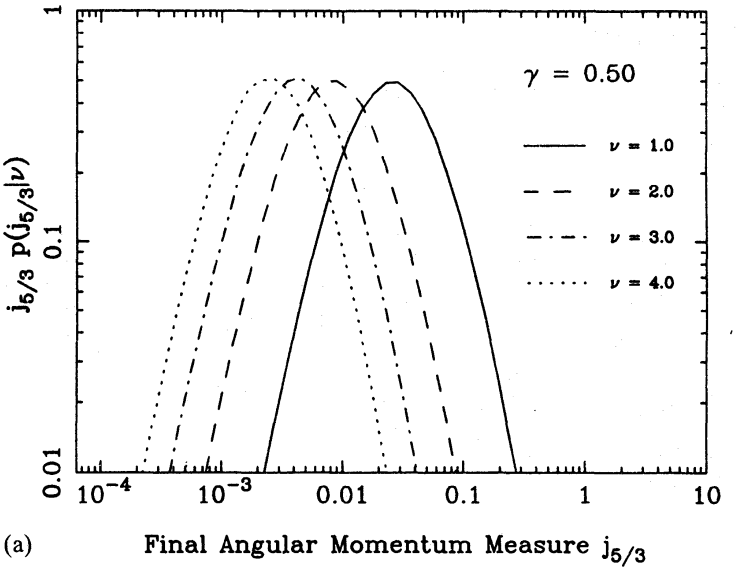

(a)

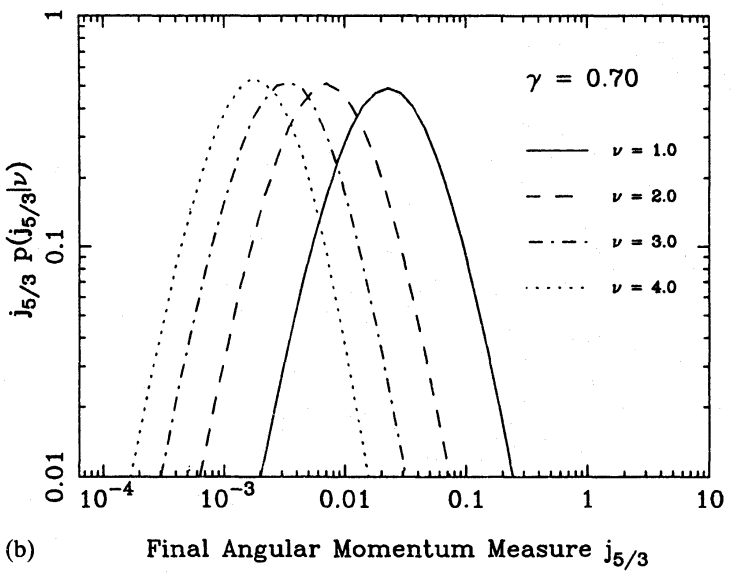

(b)

Figure 3. The distribution of final $J/M^{5/3}$. This quantity is useful for comparison with observation, because the normalization of the ordinate is independent of almost everything except one characteristic collapse epoch (equation 30). The disadvantage is that there is a very wide range in expected values of $J/M^{5/3}$. There is, however, a systematic shift to lower values for higher peaks, slightly stronger than that seen in the distribution of j (Fig. 2). This comes about because high peaks have a weak tendency to be more massive (Peacock & Heavens 1985).

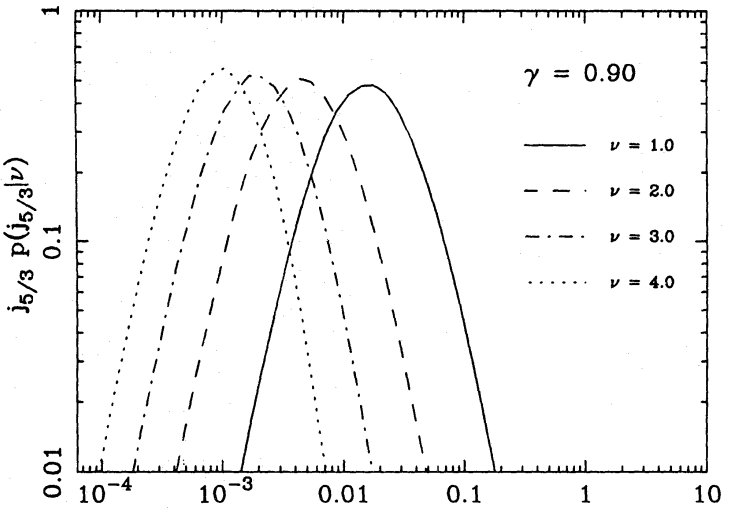

Figure 3–*continued*

individual objects are concerned – in the final stages of collapse, objects can be spun up or down, gaining or losing a significant fraction of their angular momentum. However, from the statistical point of view, this effectively amounts to broadening the *distribution* of angular momentum with respect to linear theory. Since we have already shown that linear theory predicts an extremely broad distribution, it appears likely that non-linear effects will not have an important effect on the statistical results presented here.

2.3 FINAL MASS-WEIGHTED ANGULAR MOMENTUM

In Appendix B, we also generalize the above analysis, and calculate the distributions of the final angular momentum weighted by powers of the mass: $j_a \propto J/M^a$. Apart from the specific angular momentum, characterized by the dimensionless quantity $j_1 \propto J/M$, it is most useful to calculate the quantity $j_{5/3} \propto J/M^{5/3}$:

$$j_{5/3} \equiv \frac{J}{J_{\rm ref,\,f}} \left(\frac{M}{M_{\rm ref}} \right)^{-5/3} \tag{19}$$

where $J_{\rm ref,\,f}$ comes from (15), and $M_{\rm ref} \equiv \varrho_0 R_*^3 (1-f)^{3/2}$. With these definitions, we obtain an angular momentum measure which is independent both of the loosely-determined f, and the arbitrary R_*. The independence of R_* is especially important, given that we have argued above (Section 2.1) that one may wish to consider simultaneously several values of R_*, to isolate bound systems on various scales. The universality of the $j_{5/3}$ distribution (ignoring small changes of γ with smoothing length) then means that a correlation $J \propto M^{5/3}$ is predicted in this model. A very similar correlation is indeed seen in the simulations of Barnes & Efstathiou.

The distribution of $j_{5/3}$ is shown in Fig. 3. Note that this quantity displays a marked anticorrelation with ν, in contrast to j. This probably arises partly because of the tendency of M to increase with ν (Peacock & Heavens 1985). A good fit to the $j_{5/3}$ distribution is

$$p_{\rm pk}(j_{5/3}|\nu) \cong \frac{16.3}{j_* [(j_*/j)^{2/5} + (j/j_*)^{4/5}]^5} \tag{20}$$

where the parameter j_* is fitted by

$$j_*(\gamma, \nu) = 0.01[4.8 - 3.2\nu + 0.55\nu^2 + (\gamma - 0.7)(-5.2 + 3.6\nu - 0.71\nu^2) + (\gamma - 0.7)^2(-8.4 + 5.7\nu - 1.1\nu^2)]. \tag{21}$$

2.4 FINAL SPIN PARAMETER λ

An alternative measure of angular momentum is the dimensionless spin parameter λ

$$\lambda \equiv \frac{J|E|^{1/2}}{GM^{5/2}} \tag{22}$$

where E is the total energy of the object. The final binding energy of an object is no more straightforward to calculate than final angular momentum, but can be roughly estimated by modelling our overdensity as a uniform sphere. This part of the calculation is therefore more approximate than the rest of the paper, which does not make any such simplifying assumptions. At maximum expansion, or 'turnround', the uniform sphere has a density relative to the background of approximately

$$\frac{\varrho}{\varrho_b} = \frac{9\pi^2}{16}\,\Omega_m^{-0.6} \tag{23}$$

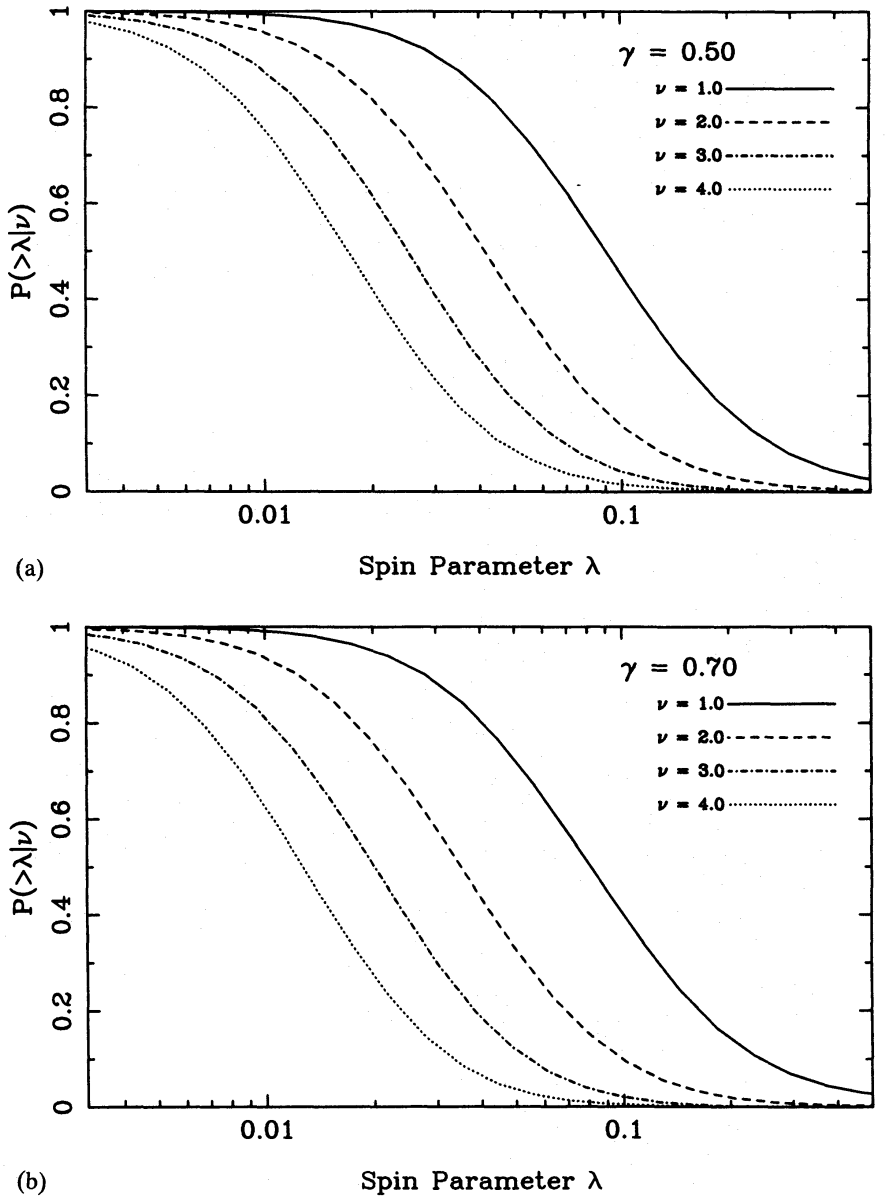

Figure 4. The distribution of final spin parameter λ (equations 22 and 28), which is related to $j_{5/3}$ (Fig. 3) by a simple scaling; this figure shows the cumulative distribution.

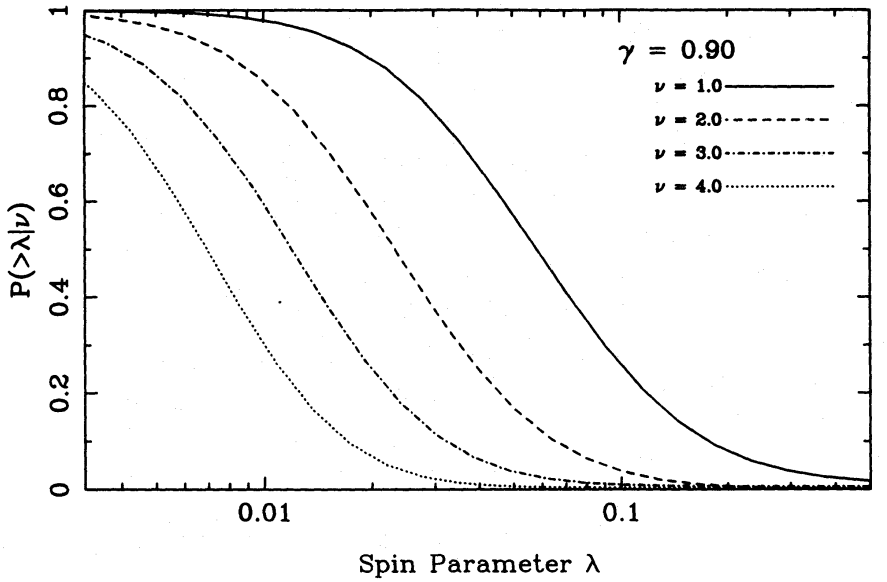

Figure 4–*continued*

(where Ω_m is the density parameter at that epoch – see equation 19.44 of Peebles 1980). At this point, the total energy is simply $3GM^2/(5r)$, where r is the sphere's proper radius. Eliminating r in terms of M and ϱ_b yields

$$|E|=\left(\frac{81\pi^3}{500}\right)^{1/3} GM^{5/3}\varrho_m^{1/3}\Omega_m^{-0.2} \tag{24}$$

(where ϱ_m is the background density at maximum). This $E \propto M^{5/3}$ correlation is seen clearly in the simulations of Barnes & Efstathiou. This yields an estimate for λ:

$$\lambda=\left(\frac{81\pi^3}{500}\right)^{1/6} G^{-1/2}JM^{-5/3}\varrho_m^{1/6}\Omega_m^{-0.1}. \tag{25}$$

Thus the distribution of $J/M^{5/3}$ effectively gives us the distribution of λ also. From equations (10) and (19), the final value of $J/M^{5/3}$ is

$$J_f M^{-5/3}=\nu^{3/2}j_{5/3}\varrho_0^{-2/3}(ag\sigma_0)_{t_c(\nu)}. \tag{26}$$

If, for simplicity, we assume that the critical time for angular momentum growth to cease occurs at turnround, then using $g(t)=a(t)H(t)\Omega^{0.6}(t)$ (Peebles 1980) and the relations between Ω, H and ϱ, we obtain the pleasingly simple result

$$\lambda=\left(\frac{384}{125}\right)^{1/6} \pi\nu^{3/2}j_{5/3}(\sigma_0)_m. \tag{27}$$

In the case of the spherical model, linear theory predicts $(\sigma_0)_m=(3/20)(6\pi)^{2/3}\nu^{-1}$ (if $\Omega_m\simeq 1$), which yields

$$\lambda=4.0\nu^{1/2}j_{5/3}. \tag{28}$$

The distribution of λ can therefore be inferred from Fig. 3. As an alternative way of presenting the information, we show the cumulative distributions of λ in Fig. 4. Despite the $\nu^{1/2}$ scaling in equation (28), λ still anticorrelates with ν; according to Appendix C, the asymptotic behaviour is $\lambda \propto \nu^{-2}$. For $\nu \sim 1$, the trend is less extreme, and the width of the distributions ensures that there is no clear separation in λ between peaks of different ν.

The values of λ displayed in Fig. 4 are very satisfactory in that the density maximum calculation has automatically yielded medians of $\lambda \simeq 0.05$, in good agreement with Barnes & Efstathiou's N-body simulations (and with the results of Hoffman 1988, who performed a similar calculation via static Monte Carlo simulation). How seriously should we take this result? We have already argued that the distribution of $JM^{-5/3}$ is very robust, being uncertain only by a factor of order unity corresponding to the precise time at which growth of J ceases. The relation for the energy (24) was derived on the basis of the spherical model, and so is only strictly correct for very high peaks. However, λ only depends on $|E|^{1/2}$, and so this uncertainty cannot affect the result very much. [Note that Hoffman's (1988) attempt to derive the energy for a general peak is flawed: he calculates the integral of the gravitational potential field minus its central value over the peak – which is *not* the same as the gravitational potential energy of the body.] In short, there is reason to believe our estimate for λ to a factor $\leqslant 2$ – the agreement with N-body simulation is not a coincidence. In particular, linear theory has been useful in identifying the *reason* for the wide spread of λ values found by Barnes & Efstathiou: equation (13) tells us that this is because the range in peak shape always induces an order of magnitude dispersion in torque.

3 Comparison with observation

As argued above, the best quantities to compare with observation are either λ or $J/M^{5/3}$. We shall argue in Section 4 that the λ values are approximately in agreement with observations for systems where dissipation has not been important. To couch the comparison in terms of $J/M^{5/3}$ directly, we need $J_{\mathrm{ref,f}} M_{\mathrm{ref}}^{-5/3}$, which is given from equation (10) by

$$\begin{aligned} J_{\mathrm{ref,f}} M_{\mathrm{ref}}^{-5/3} &= \varrho_0^{-2/3} (ag\sigma_0)_{t_c(\nu=1)} \\ &= (\varrho^{-2/3} a^{-1} g \sigma_0)_{t_c(\nu=1)} \\ &\simeq (8\pi G/3)^{2/3} (H^{-1/3}\sigma_0)_{t_c(\nu=1)} \end{aligned} \tag{29}$$

where we have assumed that $(\Omega^{2/3}\Omega^{-0.6})_{t_c(\nu=1)}$ can safely be set equal to unity. Since $H(z) = H_0(1+z)(1+\Omega_0 z)^{1/2}$ and with $H_0 \equiv 100\,h\,\mathrm{km\,s^{-1}\,Mpc^{-1}}$, $M \equiv 10^{12} M_{12}\, M_\odot$ and adopting the spherical model result for $(\sigma_0)_{t_c}$, we get

$$J = 1.0\times 10^{70}\, h^{-1/3} (1+z_1)^{-1/3} (1+\Omega_0 z_1)^{-1/6} j_{5/3} M_{12}^{5/3}\ \mathrm{kg\ m^2\ s^{-1}} \tag{30}$$

(where $\nu = 1$ peaks turn round at redshift z_1). Since the mass of a peak does generally depend on height (Peacock & Heavens 1985), there is a systematic shift of the mean value of $j_{5/3}$ to lower values for higher peaks. This may be of some use as a discriminant of peak height. It does mean, however, that the range of expected values is very large. Characteristic values are in the range 10^{-3} to 10^{-2}, with tails extending a further factor of 10 either side. Hence for z_1 not very much larger than unity, we may expect angular momenta in the range 10^{67}–$10^{68}\, M_{12}^{5/3}\,\mathrm{kg\,m^2\,s^{-1}}$.

3.1 GALAXIES

Fall & Efstathiou (1980) and Gunn (1987) argue that the dark halo matter should have the same specific angular momentum as the luminous disc material, in which case a spiral galaxy with disc scale length α^{-1} and a flat rotation curve with circular velocity v_{circ} will have angular momentum

$$J_{\mathrm{tot}} \simeq 1.0\times 10^{68}\, M_{12} \left(\frac{v_{\mathrm{circ}}}{200\ \mathrm{km\ s^{-1}}}\right)\left(\frac{\alpha^{-1}}{4\ \mathrm{kpc}}\right) \mathrm{kg\ m^2\ s^{-1}}. \tag{31}$$

Clearly tidal torques during collapse can provide a satisfactory explanation of the angular momentum of galaxies, unless the collapse redshift is very high ($z_1 > 100$, say).

3.2 CLUSTERS OF GALAXIES

For clusters of mass $10^{15} M_{15} M_{\odot}$ and half-light radius $R=R_{\rm Mpc}$ Mpc, the circular velocities implied by our analysis are of order

$$v_{\rm circ} \approx \frac{J}{MR} \approx 5 M_{15}^{2/3} R_{\rm Mpc}^{-1} \text{ km s}^{-1} \tag{32}$$

– very difficult to observe in a virialized system with large velocity dispersion. On larger scales still, Aaronson *et al.* (1982) have suggested a rotational velocity of about 180 km s^{-1} for the local supercluster. The appropriate values of M and R are rather uncertain, and the structure is very flattened (e.g. Tully 1982), but even given the wide spread in our predictions, such a velocity seems rather high. Indeed, if such a rotation were confirmed, it would present a serious challenge to the tidal torque theory for the origin of supercluster angular momentum.

4 Conclusions

We have calculated the angular momentum growth in the vicinity of local density maxima, when the density perturbations are small. We find that the distributions of angular momentum for given peak height (the peak overdensity relative to the rms) are very broad, with a systematic shift towards higher torques acting on higher peaks (opposite to the trend at $\nu \gg 1$).

However, once peaks collapse into discrete systems, angular momentum growth should be systematically reduced, as discussed by Peebles (1969), although individual objects may undergo substantial torquing of substructure (Barnes & Efstathiou 1987). Since high peaks collapse early, there is little time for the torques to act. The two opposing effects of higher torques and shorter collapse times very nearly cancel each other out, leaving us with one of the principal result of this paper: for realistic power spectra, the average angular momentum acquired by a collapsed system is independent of the height of the progenitor peak. The variation of tidal torques with peak height does depend on the power spectrum, and this determines whether high peaks acquire more or less angular momentum than the low peaks. For power spectra with large fluctuations on scales much larger than the small-scale smoothing length, peaks above a certain threshold are strongly clustered, as first pointed out by Kaiser (1984) and Politzer & Wise (1984). It is not surprising, therefore, that for such power spectra, the high peaks experience greater tidal forces. For steep power spectra, high peaks are not much more strongly clustered than the low peaks (Peacock & Heavens 1985), so the tidal torques vary much less between peaks of different height, and the collapse time is the principal determinant of final angular momentum. The changeover between torque-dominated and collapse-time-dominated behaviour occurs at about $\gamma=0.7$, which corresponds roughly to most power spectra which are currently fashionable. Cold dark matter is marginally torque-dominated, but the systematic differences between peaks of different height is rather small in comparison with the wide range of angular momenta expected for peaks of a given height.

Strictly speaking, the above results are at variance with the models of Blumenthal *et al.* (1984) and Hoffman (1986), which attempt to explain morphological trends with environment on the basis of angular momentum. They argued that high peaks, which, at least for some power spectra, are strongly clustered (see above) should acquire less angular momentum and become elliptical galaxies. This argument, although including the collapse time effect, ignores the systematic variations in tidal torques, and is only valid for very steep power spectra. However, the analysis here suggests that if the angular momentum is weighted by a power of the mass, it may act as a discriminant of peak height. The measure $J/M^{5/3}$ is useful in this regard, as its predicted values are very insensitive to cosmological parameters, and, more importantly, it does not depend on the

uncertain factor f, or on the smoothing length, which is artificially imposed in some models. We have also shown that the dimensionless spin parameter λ is proportional to $J/M^{5/3}$. The model studied here has the merit of naturally producing typical values of $\lambda \simeq 0.05$, as required both by observation and N-body simulations. Because high peaks are more massive, the λ distributions do move to lower λ for high peaks, in qualitative agreement with the arguments of Hoffman and Blumenthal *et al.* However, once again this effect is dominated by the large spread in λ at given ν (as has also been found by Hoffman 1988). It is therefore only possible to account for a weak anticorrelation of λ with ν (and hence mass). This may well be relevant to explaining the luminosity $-\lambda$ anticorrelation seen in elliptical galaxies (e.g. Efstathiou & Silk 1983), but cannot account for the fact that the discs in spiral galaxies have values of λ which are an order of magnitude higher. Any explanation for the preponderance of ellipticals in clusters therefore depends on understanding the environmental dependence of the dissipative effects which produce the high disc λ values – we cannot simply appeal to the statistical properties of the initial density field.

References

Aaronson, M., Huchra, J., Mould, J., Schechter, P. L. & Tully, R. B., 1982. *Astrophys. J.*, **258,** 64.

Abramowitz, M. & Stegun, I. A., 1965. *Handbook of Mathematical Functions,* Dover, New York.

Bardeen, J. M., Bond, J. R., Kaiser, N. & Szalay, A. S., 1986. *Astrophys. J.*, **304,** 15.

Barnes, J. & Efstathiou, G., 1987. *Astrophys. J.*, **319,** 575.

Blumenthal, G. R., Faber, S. M., Primack, J. R. & Rees, M. J., 1984. *Nature,* **311,** 517.

Couchman, H. M. P., 1987. *Mon. Not. R. astr. Soc.*, **225,** 777.

Doroshkevich, A. G., 1970. *Astrofiz.*, **6,** 581.

Efstathiou, G. & Barnes, J., 1983. In: *Formation and Evolution of Galaxies and Large Structures in the Universe, Proceedings of the Third Moriond Astrophysics Meeting,* p. 361, eds Audouze, J. & Tran Thuanh Van, J., Reidel, Dordrecht, Holland.

Efstathiou, G. & Jones, B. J. T., 1979. *Mon. Not. R. astr. Soc.*, **186,** 133.

Efstathiou, G. & Silk, J., 1983. *Fund. Cos. Phys.*, **9,** 1.

Fall, S. M. & Efstathiou, G., 1980. *Mon. Not. R. astr. Soc.*, **193,** 189.

Gunn, J., 1987. In: *The Galaxy,* eds Gilmore, G. & Carswell, B., NATO-ASI, Reidel, Dordrecht, Holland.

Hoffman, Y., 1986. *Astrophys. J.*, **301,** 65.

Hoffman, Y., 1988. *Astrophys. J.* (submitted).

Hoyle, F., 1949. In: *Problems of Cosmological Aerodynamics,* p. 195, eds Burgers, J. M. & van de Hulst, H. C., International Union of Theoretical and Applied Mechanics and International Astronomical Union, Ohio.

Ikeuchi, S., 1981. *Publs astr. Soc. Japan,* **33,** 211.

Kaiser, N., 1984. *Astrophys. J.*, **284,** L9.

More, J. G., Heavens, A. F. & Peacock, J. A., 1986. *Mon. Not. R. astr. Soc.*, **220,** 189.

Ostriker, J. P. & Cowie, L. L., 1981. *Astrophys. J.*, **243,** L127.

Peacock, J. A. & Heavens, A. F., 1985. *Mon. Not. R. astr. Soc.*, **217,** 805.

Peebles, P. J. E., 1969. *Astrophys. J.*, **155,** 393.

Peebles, P. J. E., 1980. *The Large Scale Structure of the Universe,* Princeton University Press, Princeton.

Politzer, H. D. & Wise, M. B., 1984. *Astrophys. J.*, **285,** L1.

Tully, R. B., 1982. *Astrophys. J.*, **257,** 389.

Vilenkin, A., 1985. *Phys. Repts,* **121,** 263.

White, S. D. M., 1984. *Astrophys. J.*, **286,** 38.

Appendix A: Shape and shear distribution

The angular momentum of the material in the neighbourhood of a local density maximum is obtained by making a Taylor expansion of the velocity field and the density field about the maximum. The purpose of the latter is merely to estimate the extent of the regions of high density in all directions. We must therefore consider the joint distribution of the 16 variables $\delta \equiv \delta\varrho/\varrho$, $\delta_i \equiv \partial\delta/\partial r_i$, $\delta_{ij} \equiv \partial^2\delta/\partial r_i \partial r_j$ and $v_{ij} \equiv \partial v_i/\partial r_j$, where the last two matrices have six independent components each, since they are both symmetric if we assume (curl-free) growing-mode pertur-

bations. Note that δ_{ij} is not the Kronecker delta, which does not appear in this paper. Putting the variables into a vector $\mathbf{V}$, the joint distribution for the V_i is

$$f(V_i)\ d^{16}V_i = \frac{1}{(2\pi)^8 |\mathbf{M}|^{1/2}} \exp\ [-\tfrac{1}{2}(V_i-\bar{V}_i)M_{ij}^{-1}(V_j-\bar{V}_j)]\ d^{16}V_i \tag{A1}$$

(e.g. Peacock & Heavens 1985) where $\mathbf{M}$ is the covariance matrix

$$M_{ij} = \langle (V_i-\bar{V}_i)(V_j-\bar{V}_j)\rangle \tag{A2}$$

and the bar and $\langle\ \rangle$ indicate mean values. If we define the fractional density perturbation as a Fourier transform over a (large) volume V_u:

$$\delta(\mathbf{r}) = \frac{V_u}{(2\pi)^3} \int \delta_{\mathbf{k}} \exp\ (-i\mathbf{k}\cdot\mathbf{r})\ d^3\mathbf{k},$$

$$\delta_{\mathbf{k}} = \frac{1}{V_u} \int \delta(\mathbf{r}) \exp\ (i\mathbf{k}\cdot\mathbf{r})\ d^3\mathbf{r}, \tag{A3}$$

and assume that the $\delta_{\mathbf{k}}$ have random phases and are isotropic, with amplitudes given by the power spectrum $|\delta_{\mathbf{k}}|^2$ as a function of wavenumber $k \equiv |\mathbf{k}|$, then the velocity field is given by

$$v_i = \frac{-iV_u}{(2\pi)^3} \int \frac{a}{\delta}\frac{\partial\delta}{\partial t} k_i \frac{1}{k^2} \delta_{\mathbf{k}} \exp\ (-i\mathbf{k}\cdot\mathbf{r})\ d^3\mathbf{k} \tag{A4}$$

(e.g. Peebles 1980) where $a(t)$ is the cosmic scale factor, normalized to unity at the present. The shear terms are therefore

$$v_{ij} = -g(t) \frac{V_u}{(2\pi)^3} \int \frac{k_i k_j}{k^2} \delta_{\mathbf{k}} \exp\ (-i\mathbf{k}\cdot\mathbf{r})\ d^3\mathbf{k} \tag{A5}$$

where

$$g(t) \equiv \frac{a}{\delta}\frac{\partial\delta}{\partial t} = f(\Omega)\frac{da}{dt} \approx \Omega^{0.6}\frac{da}{dt} \tag{A6}$$

using the approximation of Peebles (1980) if desired. $\Omega(t)$ is the density parameter. The non-zero correlations of the 16 variables are then

$$\langle\delta^2\rangle = \sigma_0^2$$

$$\langle\delta\delta_{11}\rangle = -\langle\delta_1\delta_1\rangle = -\sigma_1^2/3$$

$$\langle\delta v_{11}\rangle = -g\sigma_0^2/3$$

$$\langle\delta_{11}\delta_{11}\rangle = 3\langle\delta_{11}\delta_{22}\rangle = 3\langle\delta_{12}^2\rangle = \sigma_2^2/5$$

$$\langle\delta_{11}v_{11}\rangle = 3\langle\delta_{11}v_{22}\rangle = 3\langle\delta_{12}v_{12}\rangle = g\sigma_1^2/5$$

$$\langle v_{11}^2\rangle = 3\langle v_{11}v_{22}\rangle = 3\langle v_{12}^2\rangle = g^2\sigma_0^2/5 \tag{A7}$$

with obvious generalizations to other components. The σ_j are calculated from the power spectrum by

$$\sigma_j^2 \equiv \frac{V_u}{(2\pi)^3} \int |\delta_k|^2 k^{2j} 4\pi k^2\ dk. \tag{A8}$$

The inversion of the matrix M_{ij} is obtained by noting that $\langle V_i\rangle=0$, and changing variables (*cf.* Bardeen *et al.* 1986) to dimensionless forms:

$$x\equiv-(\delta_{11}+\delta_{22}+\delta_{33})/\sigma_2$$

$$y\equiv-\tfrac{1}{2}(\delta_{11}-\delta_{33})/\sigma_2$$

$$z\equiv-\tfrac{1}{2}(\delta_{11}-2\delta_{22}+\delta_{33})/\sigma_2$$

$$\nu\equiv\delta/\sigma_0$$

$$v_{\rm A}\equiv-(v_{11}+v_{22}+v_{33})/(g\sigma_0)$$

$$v_{\rm B}\equiv-\tfrac{1}{2}(v_{11}-v_{33})/(g\sigma_0)$$

$$v_{\rm C}\equiv-\tfrac{1}{2}(v_{11}-2v_{22}+v_{33})/(g\sigma_0)$$

$$w_1\equiv v_{23}/(g\sigma_0)$$

$$\tilde{\delta}_{12}\equiv\delta_{12}/\sigma_2$$

$$\tilde{\delta}_1\equiv\delta_1/\sigma_1 \qquad \text{(A9)}$$

etc. The non-zero correlations are

$$\langle x^2\rangle=\langle\nu^2\rangle=\langle v_{\rm A}^2\rangle=3\langle\tilde{\delta}_1^2\rangle=15\langle\tilde{\delta}_{12}^2\rangle=15\langle w_3^2\rangle=\langle v_{\rm A}\nu\rangle=1$$

$$\langle x\nu\rangle=5\langle v_{\rm C}z\rangle=15\langle v_{\rm B}y\rangle=15\langle\tilde{\delta}_{12}w_3\rangle=\gamma$$

$$\langle z^2\rangle=3\langle y^2\rangle=\langle v_{\rm C}^2\rangle=3\langle v_{\rm B}^2\rangle=1/5 \qquad \text{(A10)}$$

etc. where $\gamma\equiv\sigma_1^2/(\sigma_0\sigma_2)$, following the notation of Bardeen *et al.* (1986). Since $\langle v_{\rm A}\nu\rangle^2=\langle v_{\rm A}^2\rangle\langle\nu^2\rangle=1$, $v_{\rm A}$ is perfectly correlated with ν (a result which follows directly from the continuity equation) and so we may drop $v_{\rm A}$ from our system of equations. The inversion of the remaining 15×15 matrix is straightforward, as the matrix is in block-diagonal form. We have

$$|\mathbf{M}|=\frac{(1-\gamma^2)^6}{5^{10}3^{11}} \qquad \text{(A11)}$$

and $\exp(-\frac{1}{2}V_iM_{ij}^{-1}V_j)\equiv\exp(-Q_1)$, with

$$\begin{aligned}2Q_1=&\Gamma\nu^2-2\gamma\Gamma x\nu+\Gamma x^2+15\Gamma y^2-30\gamma\Gamma yv_{\rm B}+15\Gamma v_{\rm B}^2+5\Gamma z^2-10\gamma\Gamma zv_{\rm C}\\&+5\Gamma v_{\rm C}^2+15\Gamma(\tilde{\delta}_{23}^2+\tilde{\delta}_{13}^2+\tilde{\delta}_{12}^2)+15\Gamma(w_1^2+w_2^2+w_3^2)\\&-30\gamma\Gamma(\tilde{\delta}_{23}w_1+\tilde{\delta}_{13}w_2+\tilde{\delta}_{12}w_3)+3(\tilde{\delta}_1^2+\tilde{\delta}_2^2+\tilde{\delta}_3^2)\end{aligned} \qquad \text{(A12)}$$

with

$$\Gamma\equiv(1-\gamma^2)^{-1}. \qquad \text{(A13)}$$

We now restrict our attention to the principal axes of the matrix δ_{ij}. Let λ_i be the eigenvalues of $-\delta_{ij}/\sigma_2$, with $\lambda_1\geqslant\lambda_2\geqslant\lambda_3$. Following Bardeen *et al.*, we change variables from the six independent δ_{ij} to the three λ_i (note that we have normalized λ_i) and three Euler angles, representing the orientation of the principal axes. Now, Q_1 is independent of a coordinate rotation (the Jacobian of the transformation is unity for our 15-dimensional space). Thus Q_1 is independent of the Euler angles, and we may integrate over the Euler angles, giving

$$f(\nu,\delta_i,\lambda_i,v_{\rm B},v_{\rm C},w_i)=A\exp(-Q_2)|(\lambda_1-\lambda_2)(\lambda_2-\lambda_3)(\lambda_1-\lambda_3)| \qquad \text{(A14)}$$

with

$$A \equiv \frac{5^5 3^{11/2}}{2(2\pi)^{11/2}(1-\gamma^2)^3} \tag{A15}$$

and

$$2Q_2 = \Gamma\nu^2 - 2\gamma\Gamma x\nu + \Gamma x^2 + 15\Gamma y^2 - 30\gamma\Gamma y v_B + 15\Gamma v_B^2 + 5\Gamma z^2 - 10\gamma\Gamma z v_C + 5\Gamma v_C^2 + 15\Gamma(w_1^2 + w_2^2 + w_3^2) + 3(\tilde{\delta}_1^2 + \tilde{\delta}_2^2 + \tilde{\delta}_3^2) \tag{A16}$$

where

$$x = \lambda_1 + \lambda_2 + \lambda_3$$
$$y = \tfrac{1}{2}(\lambda_1 - \lambda_3)$$
$$z = \tfrac{1}{2}(\lambda_1 - 2\lambda_2 + \lambda_3). \tag{A17}$$

In the neighbourhood of a peak,

$$\frac{\partial\delta}{\partial r_i} \approx \left(\frac{\partial^2\delta}{\partial r_i \partial r_j}\right)_{pk} (r - r_{pk})_j \tag{A18}$$

so that

$$d^3\tilde{\delta}_i = \left(\frac{\sigma_2}{\sigma_1}\right)^3 |\lambda_1\lambda_2\lambda_3| \, d^3 r_i \tag{A19}$$

and we require $\lambda_3 > 0$ for a local maximum. The comoving number density of peaks in the element $d\nu \, dv_B \, dv_C \, d^3 w_i$ is

$$N_{pk} = A\left(\frac{\sigma_2}{\sigma_1}\right)^3 |\lambda_1\lambda_2\lambda_3|(\lambda_2 - \lambda_3)(\lambda_1 - \lambda_3)(\lambda_1 - \lambda_2) \exp(-Q_3) \tag{A20}$$

where

$$2Q_3 = \Gamma\nu^2 - 2\gamma\Gamma x\nu + \Gamma x^2 + 15\Gamma y^2 - 30\gamma\Gamma y v_B + 15\Gamma v_B^2 + 5\Gamma z^2 - 10\gamma\Gamma z v_C + 5\Gamma v_C^2 + 15\Gamma(w_1^2 + w_2^2 + w_3^2). \tag{A21}$$

We can integrate over v_B and v_C, as these are unconstrained, leaving

$$N_{pk} \, d\nu \, d^3\lambda_i \, d^3 w_i = \frac{B}{R_*^3} \exp(-Q_4) F(\lambda_i) \, d\nu \, d^3\lambda_i \, d^3 w_i \tag{A22}$$

where

$$F(\lambda_i) \equiv \frac{27}{2} \lambda_1\lambda_2\lambda_3(\lambda_2 - \lambda_3)(\lambda_1 - \lambda_3)(\lambda_1 - \lambda_2) \tag{A23}$$

(*cf.* Bardeen *et al.*), and

$$B \equiv \frac{3^{9/2}5^4}{2^{11/2}\pi^{9/2}(1-\gamma^2)^2}$$
$$R_* \equiv \sqrt{3}(\sigma_1/\sigma_2)$$
$$2Q_4 \equiv \nu^2 + \Gamma(x - x_*)^2 + 15y^2 + 5z^2 + 15\Gamma w^2 \tag{A24}$$

where $x_* \equiv \gamma\nu$ and $w^2 \equiv w_1^2 + w_2^2 + w_3^2$. The end result is thus a particularly simple one: the shear-

independence of Q factorizes out. It is therefore straightforward to check that the distribution is correctly normalized, by integrating over the w_i and comparing with equations A12 of Bardeen *et al.* Intuitively, this seems a reasonable outcome, as shear does not alter the density field, so one might have expected these to be independent degrees of freedom.

Appendix B: Distribution of angular momentum

We use the distribution of shapes and shears (equation A22) and the dimensionless angular momentum (equation 13) to obtain the distribution of peaks of given height and angular momentum.

It is convenient first to change variables from w_i to polar coordinates w, θ, ϕ in the obvious way. We shall calculate

$$N_{\rm pk}(j_{\rm e}, \nu)\, d\nu\, dj_{\rm e} = \int_{\lambda_i, w, \phi} N_{\rm pk}(\nu, \lambda_i, w, u \equiv \cos\theta, \phi)\, \frac{w^2\, dw\, d\phi\, d^3\lambda_i}{|\partial j_{\rm e}/\partial u|}\, d\nu\, dj_{\rm e}. \tag{B1}$$

Since the dimensionless angular momentum is

$$j_{\rm e} = \frac{2^{9/2}\pi\nu^{5/2}w}{5\times 3^{7/2}\gamma^{5/2}(\lambda_1\lambda_2\lambda_3)^{1/2}}\,[\beta^2 + (\alpha_3^2 - \beta^2)u^2]^{1/2} \tag{B2}$$

with

$$\beta^2(\lambda_i, \phi) \equiv \alpha_1^2\cos^2\phi + \alpha_2^2\sin^2\phi \tag{B3}$$

we have

$$\frac{\partial j_{\rm e}}{\partial u} = \frac{2^9\pi^2\nu^5 w^2(\alpha_3^2 - \beta^2)u}{25\times 3^7\gamma^5\lambda_1\lambda_2\lambda_3 j_{\rm e}} \tag{B4}$$

and

$$u^2 = \frac{\beta^2(w_\beta^2 - w^2)}{w^2(\alpha_3^2 - \beta^2)} \tag{B5}$$

with

$$w_\beta \equiv \frac{\Lambda^{1/2} j_{\rm e}}{K\nu^{5/2}\beta} \tag{B6}$$

where

$$K \equiv \frac{2^{9/2}\pi}{5\times 3^{7/2}\gamma^{5/2}}. \tag{B7}$$

The range of w integration is from w_β to w_3 defined by

$$w_3 \equiv \frac{\Lambda^{1/2} j_{\rm e}}{K\nu^{5/2}\alpha_3} \tag{B8}$$

and

$$\Lambda \equiv \lambda_1\lambda_2\lambda_3. \tag{B9}$$

The integration over w gives

$$I_w \equiv \left| \int_{w_3}^{w_\beta} \exp\,(-15\Gamma w^2/2) w |w_\beta^2 - w^2|^{-1/2}\, dw \right|$$

$$= \begin{cases} 2/(30\Gamma)^{1/2} \exp\,(-15\Gamma w_3^2/2)\, D(X) & \alpha_3^2 > \beta^2 \\ \pi^{1/2}/(30\Gamma)^{1/2} \exp\,(-15\Gamma w_\beta^2/2)\, erf(X) & \alpha_3^2 < \beta^2 \end{cases} \tag{B10}$$

where

$$X \equiv \left(\frac{15}{2} \Gamma |w_\beta^2 - w_3^2| \right)^{1/2} \tag{B11}$$

and

$$D(X) \equiv \int_0^X \exp\,(t^2 - X^2)\, dt \tag{B12}$$

is Dawson's integral, which has the limits $D \to X$ $(X \ll 1)$ and $D \to 1/(2X)$ $(X \gg 1)$ – see Abramowitz & Stegun (1965). The joint distribution of j_e and ν is then

$$N_{pk}(\nu, j_e) = \frac{C j_e}{R_*^3 \nu^5} \int_{\phi, \lambda_i} \frac{\exp\,(-Q_5) F(\lambda_i) \Lambda T(\alpha_3, \beta; j_e, \nu)}{\beta |\alpha_3^2 - \beta^2|^{1/2}}\, d\phi\, d^3\lambda_i \tag{B13}$$

and $T \equiv (30\Gamma)^{1/2} I_w/2$, I_w being defined by equation (B10). The normalization constant (not forgetting a factor of 2 from the mapping of $\pm u$ on to w) is

$$C = \frac{3^{11} 5^{11/2} \gamma^5 \Gamma^{3/2}}{2^{13} \pi^{13/2}} \tag{B14}$$

and

$$2Q_5 \equiv \nu^2 + \Gamma(x - x_*)^2 + 15y^2 + 5z^2. \tag{B15}$$

We can cast the integral into a more symmetric form, by replacing the ϕ integration by one over β:

$$N_{pk}(\nu, j_e) = \frac{4 C j_e}{R_*^3 \nu^5} \int_{\lambda_1=0}^{\infty} \int_{\lambda_2=0}^{\lambda_1} \int_{\lambda_3=0}^{\lambda_2} \int_{\beta=\alpha_1}^{\alpha_2} \frac{\exp\,(-Q_5) F(\lambda_i) \Lambda T(\alpha_3, \beta; j_e, \nu)}{|(\alpha_1^2 - \beta^2)(\alpha_2^2 - \beta^2)(\alpha_3^2 - \beta^2)|^{1/2}}\, d\beta\, d^3\lambda_i. \tag{B16}$$

Further integrations must be done numerically. Fig. 1 shows the angular momentum distribution for peaks of given height and given power spectrum (characterized only by γ). The points to note are the following:

(i) The angular momentum distributions are very broad.

(ii) There is a systematic shift to higher j_e for higher peaks, i.e. the torques acting on high peaks are systematically greater than the torques acting on low peaks.

(iii) The asymptotic limits are $N \propto j_e^2$ $(j_e \to 0)$, $N \propto j_e^{-7/3}$ $(j_e \to \infty)$ (see Appendix C).

B.1 FINAL ANGULAR MOMENTUM

The tidal torques act on a collapsing protosystem until it breaks away from the background and forms a discrete system. Thereafter the torques are substantially reduced (Peebles 1969) and the angular momentum ceases to grow significantly (White 1984). Note that there may subsequently be some changes in the angular momentum, particularly if the protosystems incorporate substruc-

ture (Barnes & Efstathiou 1987). We neglect any such changes, as we cannot treat them analytically, and the principal effect in the N-body simulations is to rearrange angular momentum within the structure, rather than changing the total. With these simplifications, the final angular momentum acquired during the collapse will be determined by the torques acting and the collapse time which, for an Einstein–de Sitter Universe, will be $t_c \propto \nu^{-3/2}$. Since $J \propto t$ up to this point, the final angular momentum J is characterized by normalizing to the reference angular momentum for the collapse of $1-\sigma$ peaks:

$$j \equiv \frac{J}{J_{\rm ref}[t=t_c(\nu=1)]} = j_e \nu^{-3/2}. \tag{B17}$$

This gives

$$N_{\rm pk}(\nu, j) = \frac{4Cj}{R_*^3 \nu^2} \int_{\lambda_1=0}^{\infty} \int_{\lambda_2=0}^{\lambda_1} \int_{\lambda_3=0}^{\lambda_2} \int_{\beta=\alpha_1}^{\alpha_2} \frac{\exp(-Q_5) F(\lambda_i) \Lambda T(\alpha_3, \beta; j_e, \nu)}{|(\alpha_1^2-\beta^2)(\alpha_2^2-\beta^2)(\alpha_3^2-\beta^2)|^{1/2}} \, d\beta \, d^3\lambda_i \tag{B18}$$

where j_e in T is given by equation (B17). These distributions are shown in Fig. 2. Notice that, for $\gamma=0.7$, the effect of the longer collapse times for low peaks balances the higher torques acting on the high peaks.

B.2 DISTRIBUTION OF J/M^a

If we define a reference mass

$$M_{\rm ref} \equiv \varrho_0 R_*^3 (1-f)^{3/2} \tag{B19}$$

then the distribution of

$$j_a \equiv \frac{J}{J_{\rm ref,\,f}} \left(\frac{M}{M_{\rm ref}} \right)^{-a} \tag{B20}$$

is obtained by noting that the mass associated with a peak is

$$M = \frac{4\pi}{3} \varrho_0 a_1 a_2 a_3 = \frac{2^{7/2} \pi \nu^{3/2}}{3^{5/2} \gamma^{3/2} \Lambda^{1/2}} M_{\rm ref} \tag{B21}$$

using equation (6), so

$$j_a = \left(\frac{3^5 \gamma^3}{2^7 \pi^2} \right)^{a/2} j \nu^{-3a/2} \Lambda^{a/2}. \tag{B22}$$

The distributions of j_a are obtained in exactly the same way as equation (B16), resulting in

$$N_{\rm pk}(\nu, j_a) = \frac{4C_a j_a}{R_*^3 \nu^{2-3a}} \int_{\lambda_1=0}^{\infty} \int_{\lambda_2=0}^{\lambda_1} \int_{\lambda_3=0}^{\lambda_2} \int_{\beta=\alpha_1}^{\alpha_2} \frac{\exp(-Q_5) F \Lambda^{1-a} T(\alpha_3, \beta; j_e, \nu)}{|(\alpha_1^2-\beta^2)(\alpha_2^2-\beta^2)(\alpha_3^2-\beta^2)|^{1/2}} \, d\beta \, d^3\lambda_i \tag{B23}$$

where

$$C_a \equiv C \left(\frac{2^7 \pi^2}{3^5 \gamma^3} \right)^a \tag{B24}$$

and the j_e in T is

$$j_e = j_a \left(\frac{2^7 \pi^2}{3^5 \gamma^3} \right)^{a/2} \nu^{3(1+a)/2} \Lambda^{-a/2}. \tag{B25}$$

Appendix C: Asymptotic limits

This appendix considers the form of the probability distribution $p(j_a, \nu)$ in the limits $j_a \to 0$, $j_a \to \infty$ and $\nu \to \infty$.

(i) $j_a \to 0$.

This case is straightforward, since the only j_a dependence in the integral in equation (B23) is carried by T: from equation (B10) we see that $T \propto j_a$ for $j_a \ll 1$, and hence

$$p(j_a, \nu) \propto j_a^2 \tag{C1}$$

for all a, ν, γ.

(ii) $j_a \to \infty$.

This case is more complex, and it is better to go back to the definition of j_e (equation 13). Since very high values of w_i are exponentially improbable, the only way of obtaining large values of j_e is if one or more of the λ_i become close to zero. Now, equations (A22) and (A23) tell us that the probability of having two of the λ_i very small is negligible by comparison with the probability of just one (λ_3 by the ordering) being small. In this case, the λ_3 dependences of the relevant quantities are

$$j \propto \lambda_3^{-3/2}$$

$$M \propto \lambda_3^{-1/2}$$

$$j_a \propto jM^{-a} \propto \lambda_3^{(a-3)/2}$$

$$dN_{pk} \propto \lambda_3 \, d\lambda_3. \tag{C2}$$

So, eliminating λ_3 in terms of j_a, we obtain

$$p(j_a, \nu) \propto j_a^{(7-a)/(a-3)}, \tag{C3}$$

i.e. slopes of $j^{-7/3}, j_1^{-3}, j_{5/3}^{-4}$. This argument clearly breaks down for $a \geqslant 3$, when the objects of high j_a are of *low* mass.

(iii) $\nu \to \infty$.

Very high peaks become spherical, so we may expect that they would experience smaller torques. To show this, consider equations (A23) and (A24): these tell us that, for very high ν,

$$\lambda_i = \frac{\gamma\nu}{3} + \varepsilon_i \tag{C4}$$

where the ε_i are of order unity. If we rewrite equation (13) to first order in $\varepsilon_i/\gamma\nu$, we obtain

$$j_e = \frac{2^{9/2}\pi}{5\gamma^6\nu} (\Delta_1^2 w_1^2 + \Delta_2^2 w_2^2 + \Delta_3^2 w_3^2)^{1/2} \tag{C5}$$

where $\Delta_1 \equiv \varepsilon_2 - \varepsilon_3$, etc. Note that, to this order, we are able to replace Λ by $(\gamma\nu/3)^3$. In this limit ($\gamma\nu/3 \gg 1$), the relation with j_a (equation B25) is especially simple:

$$j_a = \left(\frac{3\gamma^3}{2^{7/2}\pi}\right)^a j_e \nu^{-3/2}. \tag{C6}$$

Thus, for very high peaks, we have the asymptotic behaviour $j_e \propto \nu^{-1}$, $j_a \propto \nu^{-5/2}$. A comparison with

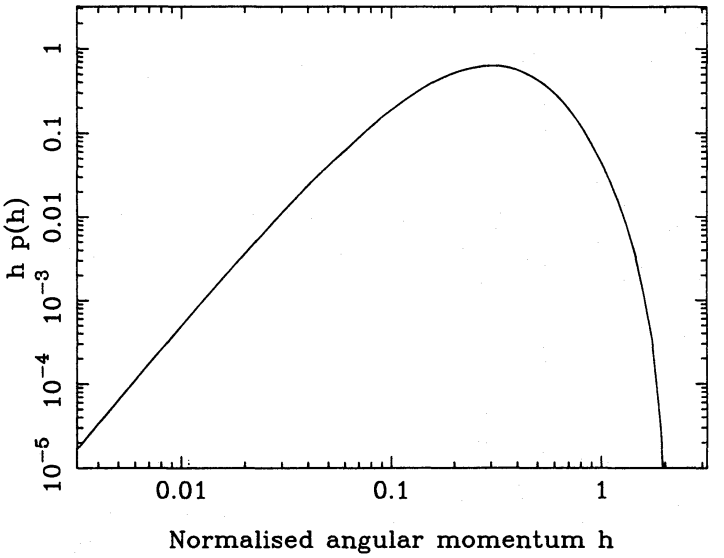

Figure C1. The distribution of 'normalized dimensionless' angular momentum h, in the high peak limit (equation C7).

Figs 1 and 2 shows that this behaviour differs considerably from that displayed for values of ν of practical relevance ($\nu<4$): j_e tends to *increase* with ν over this range.

Finally, we give the distribution of j_a in the high-peak limit. For this, we need to know only the distribution of the second factor in (C5), which clearly scales as $\Gamma^{1/2}$. Thus, there is a universal asymptotic distribution in terms of h, where

$$j_e \equiv \frac{2^{9/2}\pi}{5\gamma^6\nu}\Gamma^{1/2}h. \tag{C7}$$

The distribution of h can be obtained via a slight modification of the procedure in Appendix B, and is illustrated in Fig. C1. A very good fit (accurate to a few per cent for $h\leqslant 2$) is given by

$$p(h)=563\,h^2\exp\left[-12\,h+2.5\,h^{1.5}+8-3.2(1500+h^{16})^{1/8}\right]. \tag{C8}$$

This asymptotic form is close to the exact result for $\gamma=0.9$, $\nu=4$, and therefore may be a useful approximation in general for $\gamma\nu>4$. Note that the high-h form of equation (C7) is not a power-law: the distribution will break to a power-law only when the $\lambda_i\simeq\gamma\nu/3$ approximation breaks down, i.e. when $h\geqslant\gamma\nu$.